



Full Length Article

Parallel *in vitro* ion channel and *in vivo* zebrafish assaying of elapid snake venoms following chromatographic separation of toxin components

Arif Arrahman^{a,b,f} , Haifeng Xu^{a,b}, Muzaffar A. Khan^{c,g}, Tijmen S. Bos^{a,b}, Julien Slagboom^{a,b} , Guus C. van der Velden^c, Ulrike Nehrlich^c, Nicholas R. Casewell^d, Michael K. Richardson^c, Christian Tudorache^c, Fernanda C. Cardoso^e, Jeroen Kool^{a,b,*} 

^a Amsterdam Institute of Molecular and Life Sciences (AIMMS), Division of Bioanalytical Chemistry, Department of Chemistry and Pharmaceutical Sciences, Faculty of Sciences, Vrije Universiteit Amsterdam, Amsterdam, The Netherlands

^b Centre for Analytical Sciences Amsterdam (CASA), The Netherlands

^c Institute Biology Leiden, Leiden University, Leiden, The Netherlands

^d Centre for Snakebite Research and Interventions, Department of Tropical Disease Biology, Liverpool School of Tropical Medicine, Liverpool, United Kingdom

^e Institute for Molecular Bioscience, The University of Queensland, Brisbane, Australia

^f Faculty of Pharmacy Universitas Indonesia, Depok, Jawa Barat, Indonesia

^g Department of Microbiology and Molecular Genetics, Bahauddin Zakariya University, Multan, Pakistan

ARTICLE INFO

Keywords:

Elapid snake venom
zebrafish *in vivo* assay
ion channel *in vitro* assays
mass spectrometry
nanofractionation
toxicity assay
proteomics

ABSTRACT

Snake venoms are complex bioactive mixtures designed to paralyse, kill, or digest prey. These venoms are of pharmacological interest due to their ability to modulate molecular targets such as ion channels and receptors with high specificity and potency. Traditional studies often focus on *in vitro* molecular analysis or *in vivo* behavioural effects, limiting comprehensive understanding. Here, we present a high-throughput screening platform that combines *in vitro* ion channel assays with *in vivo* zebrafish larval bioassays using nanofractionation analytics. This method integrates post-column calcium flux assays, zebrafish paralytic bioassays, toxin mass spectrometry, and proteomics to link bioactivity with toxin identification. Using elapid snake venoms (genus *Dendroaspis*, *Naja*, and *Hemachatus*) as a proof of concept, we identified several toxins modulating ion channels with paralytic effects on zebrafish larvae. Our approach enables parallel acquisition of *in vitro* and *in vivo* data, offering a robust guide for identifying and characterising ion channel modulators with defined molecular targets.

1. Introduction

Snake venoms are complex bioactive mixtures mainly comprising proteins and peptides secreted in the venom glands of venomous snake species. The primary purpose of venom is for paralysing, killing and potentially predigesting prey, but it also has defensive purposes, such as in the context of human snakebite [1,2]. Many venom toxins are highly active compounds capable of inflicting pathological responses in prey and in snakebite victims [3,4]. The functional activity of such compounds can be diverse, and include neurotoxins [5,6], which can affect gated ion channel functioning [7], hemotoxins, which can interfere with the coagulation cascade and cause haemolysis and haemorrhage [8,9], and cytotoxins, which can destroy cells and tissues [10].

Current pharmaceutical research on venom is often directed toward the potential medicinal use of individual toxins in venoms. This research

can be referred to as venoms-to-drugs pipelines, where toxins are profiled in a targeted fashion, with ion channels comprising important targets [11–13]. Many venoms contain neurotoxins that disrupt neuromuscular transmission mediated by ion channels to paralyse envenomed prey rapidly [14]. Some of these ion channel targets involved in the resulting highly pathological processes are also drug targets [15]. Due to the high specificity and potency of many venom toxins, they have become an invaluable source for modulating a wide range of new and validated drug targets. Snake venom neurotoxins primarily target the neuromuscular junction (motor end plate) of skeletal muscle. This junction consists of the motor nerve terminal or bouton on the pre-synaptic side, and the nicotinic acetylcholine receptor (nAChR; an ion channel) on the post-synaptic side. In severe neurotoxic envenoming, neuromuscular paralysis will eventually involve severe limb muscle paralysis, and lung muscle paralysis causing respiratory collapse [16].

* Corresponding author.

E-mail address: j.kool@vu.nl (J. Kool).

<https://doi.org/10.1016/j.slasd.2025.100239>

Received 6 March 2025; Received in revised form 30 April 2025; Accepted 5 May 2025

Available online 5 May 2025

2472-5552/© 2025 The Authors. Published by Elsevier Inc. on behalf of Society for Laboratory Automation and Screening. This is an open access article under the CC BY license (<http://creativecommons.org/licenses/by/4.0/>).

Although the toxin target nAChR is well characterised, only a few of the toxins responsible for the paralysis have been identified. Prominent examples include members of the α -neurotoxins and β -neurotoxins, with α - and β -bungarotoxins from the elapid snake genus *Bungarus* the most well-known [17].

Venom separation employing one or two-dimensional liquid chromatography and high-throughput *in vitro* screening assays, mostly targeting ion channels, is the next step in drug development from venom libraries [18–21]. *In vitro* calcium flux assays are used in venom-based ion channel drug discovery [22]. These *in vitro* methods allow high throughput ion channel specificity, potency, and signalling modulation testing. At an early stage, the most fascinating toxins are identified and their modulations are examined at the molecular level to determine ion channel selectivity and interactions involved in the observable behaviour [23]. High-throughput pharmaceutical screens can be fully automated using these *in vitro* assays [24]. These can uncover and define very potent compounds that regulate the desired effect *in vitro*, but they do not reveal the pharmacological action in the complete organism. In addition, characterising the molecular target function of discovered toxins before the biological response generally leads to many compound falling short *in vivo* [25].

Therefore, fast response *in vivo* research can be preferable and whole organismal effects are directly measured using purified venom peptides. However, this is often a very low throughput and costly endeavour, and it raises ethical issues with experimental animals, limiting the number of *in vivo* studies characterizing venom peptides. For these *in vivo* studies alone, the molecular targets that are modulated stay unknown, and relatively large quantities of toxins are required. In short, it can be assessed if the venom toxins have the desired pharmaceutical effects, but the specific target(s) these compounds are modulating cannot be determined at this stage.

Reversed-phase liquid chromatography with a fraction module and mass spectrometry (RPLC-MS) has improved snake venom component separation [26]. This innovative technology isolates and analyses venom peptides and proteins with excellent resolution and sensitivity. RPLC-MS provides mass and structural data for venom components identification. This approach efficiently separates complicated venom mixtures into individual venom components for *in vitro* bioassaying when combined with a fractionation module. This approach improves venom component identification and streamlines biological activity testing [27,28]. Targeted antivenom therapies and venom-derived bioactive chemical research requires this methodological breakthrough. Multiple bioactive toxins work synergistically on many different targets because crude venoms are complex mixtures. This prohibits the bioactivities of individual toxins from being assessed at the crude venom level, and the cumulative effect of all toxins in venoms is typically destructive to *in vitro* cellular assays and lethal in *in vivo* assays. When studying bioactive toxins in venoms, these toxins must be isolated. Which pure toxin generates a specific bioactivity determined by any bioassay is unknown without chemical characterisation like proteomics analysis. Therefore, after separation, chemical analysis must be done alongside bioassay.

In vivo and *in vitro* analysis in parallel would provide both the molecular target information in combination with whole-organism effects readout. Usually, this would not be feasible as the *in vivo* experimental animal studies are too low throughput to be combined with the *in vitro* HTS ion channel assays. In that regard, recent advances in higher throughput *in vivo* assays, such as zebrafish embryo assays, can be implemented in parallel with the *in vitro* targeted workflow. This can provide a better understanding of the screening of venom toxins at the molecular level while simultaneously obtaining *in vivo* pharmacological information on the eventual effect in the whole organism. Zebrafish embryo (*Danio rerio*) larvae allow high throughput assays, which can be conducted in a 96-well format. Although zebrafish are more distantly related to humans than are rodent models, their receptors targeted by venom toxins are highly conserved [29,30], leading to a good compromise between model validity and throughput [31–33]. Further, this *in*

in vivo system enables relevant biological behaviours such as paralysis and pain induced by venom toxins to be monitored. The zebrafish larvae model thus offers a relatively low-cost and high-throughput option for assays to measure the *in vivo* effects of venom toxins.

In this study, we demonstrate an innovative profiling platform (Fig. 1) integrating liquid chromatography, high-resolution nanofractionation, and bioassaying with parallel chemical analysis of toxins through MS detection. We employed post-separation bioassays using *in vitro* calcium flux assays and *in vivo* zebrafish assays for comprehensive characterization of venom toxins in different elapid snake venoms from *Dendroaspis polylepis* (black mamba), *Naja pallida* (red spitting cobra), and *Hemachatus haemachatus* (rinkhals). Additional work was also performed on the venoms of related species, specifically *Dendroaspis angusticeps* (eastern green mamba), *Dendroaspis viridis* (western green mamba), *Naja naja* (spectacled cobra), *Naja mossambica* (Mozambique spitting cobra), and *Naja haje* (Egyptian cobra). Our results provide insights into the effects of venom toxins on ion channels and *in vivo* physiological behaviour, while simultaneously providing the identity of venom components exerting the bioactivities.

2. Material and Methods

2.1. Pipeline description

The methodological approach first separated the venom components using chromatography. After the chromatographic separation, a flow splitter (9:1 [v/v]) was used to direct the larger portion of the split flow to a nanofractionation device for high-resolution fractionation, as also described by Arrahman and Still *et al.* for enzymatic and coagulation activity bioassaying [34,35]. The smaller eluate portion was directed to UV and MS detection to obtain information for identifying the fractionated toxins. High-resolution fractions were collected into 48 or 96-well plates using a FractioMate™ nanofractionation module. Subsequently, well plates were vacuum centrifuged to dryness. Next, plates with dried venom toxins were subjected to either *in vitro* high throughput calcium flux assays or *in vivo* zebrafish assays. Thus, the venom toxins after separation were used for (1) ion channel functional assays, (2) zebrafish toxicity assays, and (3) zebrafish paralysing assays, to find *in vivo* effects and respective molecular targets. This way, toxins that interact with ion channel(s) and their *in vivo* physiological effect(s) on the organism can be investigated. It allows for correlating *in vivo* behaviour effects with molecular target ion channel identification. In this study, the venoms of *Dendroaspis polylepis*, *Naja pallida*, and *Hemachatus haemachatus* (discussed in the main text; see Tables 1–2). *Dendroaspis angusticeps*, *Dendroaspis viridis*, *Naja naja*, *Naja mossambica*, and *Naja haje* (see S Figures 1–5; S Table 1) were profiled.

2.2. Chemical and Biological Reagents

A Milli-Q Plus System (Millipore, Amsterdam, The Netherlands) was used for purifying the water used in this study. Acetonitrile (ACN, UPLC/MS grade) was obtained from Concord NC, USA. Formic acid (FA, MS grade) and acetic acid (AA) were purchased from Biosolve (Valkeniswaard, The Netherlands). NaCl, KCl, CaCl₂·2H₂O, MgSO₄·7H₂O, and ammonium bicarbonate were analytical grade and purchased from Merck (Kenilworth, UK). Methylene blue (reagent grade) was purchased from Sigma-Aldrich, Darmstadt, Germany. The zebrafish embryo medium was made by dissolving 2.94 g of NaCl, 0.13 g of KCl, 0.49 g of CaCl₂·2H₂O, 0.81 g of MgSO₄·7H₂O, and 10 g of methylene blue into 10 L of water. B-mercaptoethanol and Iodoacetamide were purchased from Sigma-Aldrich, Darmstadt, Germany. Lyophilised trypsin Gold™ (mass spectrometry grade) enzyme was purchased from Promega Corporation, Madison, USA. The trypsin was reconstituted in 50 mM acetic acid to obtain a 1 µg/µL concentration, which was aliquoted and stored at -80°C until use.

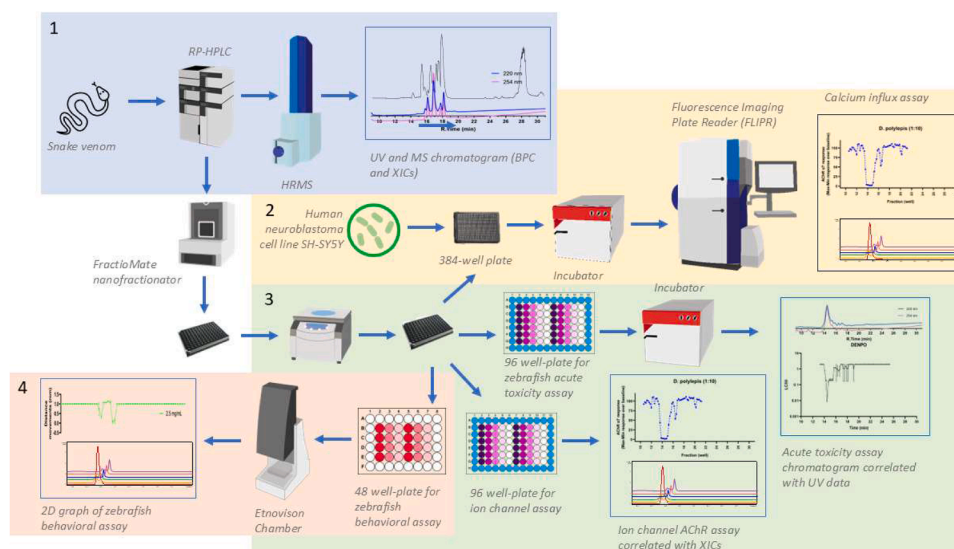


Fig. 1. Schematic overview of the complete analytical, biochemical and biological bioassaying workflow. Four main experiments run simultaneously in this study: (1) venom separation and mass spectrometry detection (using reversed-phase high-performance liquid chromatography-tandem mass spectrometry, RP-HPLC-MS), resulting in LC-UV and MS data. Via a post-column flow-split, toxins are also fractionated in high resolution using the nanofractionation analytics approach. The fractionated toxins (on well plates) can then either be analysed by proteomics (resulting in toxin identifications) or be assessed biochemically and biologically by: (2) *in vitro* $\alpha 7$ nicotinic acetylcholine receptor or L-type calcium channel calcium influx assays (resulting in ion channel bioassay chromatograms); (3) zebrafish lethality toxicity assays (resulting in LD₅₀ bioassay chromatograms); (4) *in vivo* zebrafish paralyzing bioassays (resulting in paralyzing bioassay chromatograms).

2.3. Venom Preparation

The venom used was from the following snake species: Black Mamba (*Dendroaspis polylepis*, Tanzania), Eastern Green Mamba (*Dendroaspis angusticeps*, Tanzania), Western Green Mamba (*Dendroaspis viridis*, Togo), Indian Cobra (*Naja naja*, captive-bred), Red Spitting Cobra (*Naja pallida*, Tanzania), Black-necked Spitting Cobras (*Naja nigricollis*, Tanzania), Egyptian Cobra (*Naja haje*, Uganda), and Rinkhals (*Hemachatus haemachatus*, South Africa). Lyophilised venoms, pooled from multiple animals, were provided by the Snakebite Research and Interventions Herpetarium (Liverpool School of Tropical Medicine, UK) or from the historical VU venom library (Vrije Universiteit Amsterdam, The Netherlands). The lyophilised venoms were stored long-term at -80°C . The stock solutions of the crude venoms (10.0 ± 0.1 mg/mL) were prepared in water and then aliquoted and stored at -80°C until use.

2.4. Venom Fractionation and Mass Spectrometry

Separation of venom toxins from the crude venoms injected was carried out by liquid chromatography (LC) followed by a flow splitter directing 10% of the eluent to mass spectrometry (MS) and 90% to high-resolution fractionation on well plates for subsequent post-column bioassaying or proteomics analyses. A 50 μL 10 mg/mL venom sample was injected with a Shimadzu SIL-20A autosampler for LC separation performed by an LC system controlled via Shimadzu LabSolutions software. The analytical gradient was performed by a binary Shimadzu LC-30AB pump (A and B) at a total flow rate of 0.5 mL/min. Mobile phase A was water-acetonitrile (ACN)-formic acid (FA) (98:2:0.1, v/v/v) and mobile phase B was water-ACN-FA (2:98:0.1, v/v/v). The following gradient was used: 0% to 10% B (10 min), 10% to 95% B (20 min), 95% B (2 min), 95% to 0% B (2 min). Equilibration for 5 min. A 100 \times 4.6 mm ID analytical column packed with Xbridge BEH300 reversed-phase C18 material (3.5 μm) was used for separation. The column eluate was split in a 1:9 ratio using a T-piece low-dead-volume flow splitter. The smaller flow part after the split (0.05 mL/min) was directed via a Shimadzu SPD 20A UV-Vis detector with dual-wavelength (220 and 254 nm, these wavelengths were selected as they correspond to peptide bond absorption, 220 nm, and aromatic amino acids, 245 nm), commonly used for

protein detection) measurement to a Bruker Maxis HD Mass Spectrometer (Bruker Daltonics, Bremen, Germany). For mass analysis, the Maxis HD mass spectrometer was equipped with an electrospray ionisation source (ESI) and operated in positive ion mode. The parameters of the ESI source were source temperature 200°C ; capillary voltage 4500 V; dry gas flow 4.0 L/min; mass range 500-3000 m/z with a data-sampling time of 1 s. Protein masses (Da) were calculated using the Data Analysis 5.0 (Bruker, Darmstadt, Germany). The larger eluate flow part of the split was fractionated (12 s/well) in serpentine fashion onto black 96 well plates (Greiner Bio-One, Alphen aan den Rijn, The Netherlands) by use of a FractioMate™ FRM100 nanofractionation collector (Vrije Universiteit Amsterdam, The Netherlands) controlled by FractioMator software. The outer wells of the well plate were excluded for fractionation. After nanofractionation, the plates were vacuum centrifuged overnight to dryness at room temperature using a Christ Rotational Vacuum Concentrator RVC 2-33 CD Plus (Salm en Kipp, Breukelen, The Netherlands) with an integrated cooling trap operating at -80°C . The plates were stored at -80°C .

2.5. Proteomics Analysis

For proteomics analysis, an Ultimate 3000 nano HPLC module (Thermo Scientific, Massachusetts, USA) coupled with Bruker TIMS-TOF Mass Spectrometer (Bruker Daltonics, Bremen, Germany) was used. Samples were injected with a WPS-3000(RS) autosampler, and nanoLC separations were performed with a nanoLC system controlled via Chromeleon 7.2 SR4 MUB software. The gradient was set using a nano-LC binary pump (A and B) at a total flow rate of 0.5 $\mu\text{L}/\text{min}$. Mobile phase A was water-FA (100:0.1 v/v), and mobile phase B was water-ACN-FA (20:80:0.1, v/v/v). The system was also equipped with a loading pump, for which the solvent water-ACN-FA (99:1:0.05 v/v/v) was used. The following gradient was used: 1% B (10 min), 1% - 20% B (5 min), 20% - 50% B (30 min), 50% - 85% B (1 min), 85% B (5 min) 85% - 1% B (0.5 min), 1% B (9.5 min). For sample trapping, an Acclaim PepMap 100 reversed-phase C18 trapping column (particle diameter 5 μm and column dimensions of 5 \times 0.3 mm) was used. An Acclaim PepMap 100 reversed-phase C18 analytical column (particle diameter 2 μm and column dimensions of 150 \times 0.75 mm) was used to separate the

Table 1

Overview of analysed venoms and bioactivity peaks. A comprehensive data summary for chemical venom fraction analysis and bioassays is given in the table. The table gives for each venom analysed the retention time of fractionated and post-column analysed toxins, the summarized *in vitro* and *in vivo* bioassay responses measured, and toxin accurate masses measured next to toxin identification by proteomics.

Species	R. Time (min)	LD ₅₀ assay (negative peaks)	nAChR α 7 Calcium influx assay (negative peaks)	nAChR α 7 activator assay (positive peaks)	L-type channel assay (negative peaks)	L-type channel activator assay (positive peaks)	Paralysing assay (negative peaks)	Accurate Mass (Da)	Protein Identification
<i>Dendroaspis polylepsis</i>	13.8	N.A.	Response: -0.8 % (1:10) 68.6 % (1:50) 90.9 % (1:250)	N.A.	Response: 89.2 % (1:10) 88.1 % (1:50)	N.A.	No paralysis	8010.61	3L21_NAJOX (Alpha-elapitoxin-Nno2a) <i>Naja oxiana</i>
	14.4	LD ₅₀ : 0.19 μ g/mL	Response: -2.6 % (1:10) 29.1 % (1:50) 79.7 % (1:250)	N.A.	Response: 90.7 % (1:10) 87.9 % (1:50)	N.A.	27 % paralysis	N.A.	N.A.
	14.6	LD ₅₀ : 0.009 μ g/mL	Response: -2.5 % (1:10) 23.9 % (1:50) 64.0 % (1:250)	N.A.	Response: 91.7 % (1:10) 87.5 (1:50)	N.A.	69 % paralysis	7129.47	VKTA_MICTN (Kunitz-type neurotoxin MitTx-alpha) <i>Micrurus tener</i>
	15.0	LD ₅₀ : 0.16 μ g/mL	Response: -2.3 % (1:10) 73.2% (1:50) 67.2 % (1:250)	N.A.	Response: 85.4 (1:10) 83.33 % (1:50)	N.A.	No paralysis	6555.20	VKTHK_DENPO (Kunitz-type serine protease inhibitor homolog dendrotoxin K (Fragment)) <i>Dendroaspis polylepsis</i>
	15.2	LD ₅₀ : 0.21 μ g/mL	Response: 4.02 % (1:10) 85.8 % (1:50) 72.6 % (1:250)	Response: 4.6 % (1:10)	Response: 83.0 % (1:10) 85.8 % (1:50)	N.A.	No paralysis	6549.84	3SXQ_OPHHA (Short neurotoxin SNTX26) <i>Ophiophagus hannah</i>
	15.6	LD ₅₀ : 0.21 μ g/mL	Response: 30.9 % (1:10) 80.5 % (1:50) 78.7 % (1:250)	Response: 73.3% (1:10)	Response: 87.6 % (1:10) 91.1 % (1:50)	N.A.	100 % Full paralysis	7040.14	3SLS_DENPO (Calciseptin) <i>Dendroaspis polylepsis polylepsis</i> D_polylepsis_T0010_3FTx
	16.4	LD ₅₀ : 0.21 μ g/mL	Response: 51.9 % (1:10) 84.7 % (1:50) 68.4 % (1:250)	Response: 2 % (1:10)	Response: 89.3 % (1:10) 80.7 % (1:50)	N.A.	No paralysis	7982.64	3L24_DENPO (Alpha-elapitoxin-Dpp2d) <i>Dendroaspis polylepsis</i>
	16.2	LD ₅₀ : 1.06 μ g/mL	Response: 75.7 % (1:10) 92.1 % (1:50) 97.9 % (1:250)	Response: 100 % (1:10)	Response: 84.7 % (1:10) 83.2 % (1:50)	N.A.	No paralysis	8532.97	Three-finger toxin
	16.4	LD ₅₀ : 0.95 μ g/mL	Response: 44.9 % (1:10) 65.4 % (1:50) 16.4 % (1:250)	N.A.	Response: 90.1 % (1:50) 85.3 % (1:50)	N.A.	No paralysis	7982.68	3L24_DENPO (Alpha-elapitoxin-Dpp2d) <i>Dendroaspis polylepsis</i>
	16.8	LD ₅₀ : 0.95 μ g/mL	Response: 89.3 (1:10) 95.3 % (1:50) 90.9 % (1:250)	N.A.	Response: 81.9 % (1:10) 73.9 % (1:50)	N.A.	No paralysis	7377.36	3SIM3_DENAN (Muscarinic toxin 3) <i>Dendroaspis angusticeps</i>
	17.2	N.A.	Response: 92.9 % (1:10) 94.6 % (1:50) 80.5 % (1:250)	N.A.	Response: 89.9 % (1:10) 60.8 % (1:50)	N.A.	No paralysis	7572.18	3NO28_NAJNA (Weak neurotoxin 8) <i>Naja naja</i>
	17.6	LD ₅₀ : 1.06 μ g/mL	Response: 91.6 % (1:10) 89.7 % (1:50) 87.7 % (1:250)	N.A.	Response: 88.7 % (1:10) 87.9 % (1:50)	N.A.	No paralysis	6481.97	VKT4_PSETT (Kunitz-type serine protease inhibitor textilinin) <i>Pseudonaja textilis</i>
	18.0	LD ₅₀ : 1.06 μ g/mL	Response: 93.8 % (1:10) 94.2 % (1:50) 95.8 % (1:250)	N.A.	Response: 84.3 % (1:10) 82.5 % (1:50)	N.A.	No paralysis	8284.96	Three-finger toxin
<i>Naja pallida</i>	15.2	LD ₅₀ : 1.12 μ g/mL	Response: 76.3 % (not	N.A.	N.A.	N.A.	No paralysis	6901.42	3SA6_NAJAT (Cytotoxin 6) <i>Naja atra</i>

(continued on next page)

Table 1 (continued)

Species	R. Time (min)	LD ₅₀ assay (negative peaks)	nAChR α 7 Calcium influx assay (negative peaks)	nAChR α 7 activator assay (positive peaks)	L-type channel assay (negative peaks)	L-type channel activator assay (positive peaks)	Paralysing assay (negative peaks)	Accurate Mass (Da)	Protein Identification
	16.6	LD ₅₀ : 0.44 μ g/mL	diluted) 77.8 % (1:10) Response: 45.1 % (not diluted)	N.A.	N.A.	N.A.	95 % paralysis	6732.29	3S12_NAJNA (Alpha-elapitoxin-Nn2a) <i>Naja naja</i> 3SA7A_NAJKA (Cytotoxin 2) <i>Naja kaouthia</i>
	17.2	LD ₅₀ : 0.45 μ g/mL	91.0 % (1:10) Response: 94.2 % (not diluted)	N.A.	N.A.	N.A.	No paralysis	6782.34	3S11_NAJPA (Short neurotoxin 1) <i>Naja pallida</i>
	17.4	LD ₅₀ : 0.45 μ g/mL	95.6 % (1:10) Response: 91.7 % (not diluted)	N.A.	N.A.	N.A.	69 % paralysis	6948.36	3S1CB_NAJNA (Cobrotoxin homolog) <i>Naja naja</i>
	17.4	LD ₅₀ : 0.0895 μ g/mL	Response: 86.3 % (1:10) 89.6 % (not diluted)	N.A.	N.A.	N.A.	No paralysis	6883.39	3SA3_NAJMO (Cytotoxin 3) <i>Naja mossambica</i>
	18.2	LD ₅₀ : 0.0179 μ g/mL	92.5 % (1:10) Response: 88.1 % (not diluted)	N.A.	N.A.	N.A.	4 % paralysis	6815.31	3SA1_NAJPA (Cytotoxin 1) <i>Naja pallida</i>
<i>Hemachatus haemachatus</i>	15.4	LD ₅₀ : 0.18 μ g/mL	92.9 % (1:10) Response: 79.2 % (not diluted)	N.A.	N.A.	N.A.	No paralysis	7091.10	3SUB_DENAN (Muscarinic toxin) <i>Dendroaspis angusticeps</i>
	15.8	LD ₅₀ : 0.04 μ g/mL	86.6 % (1:10) Response: 63.5 % (not diluted)	N.A.	N.A.	N.A.	3 % paralysis	7208.50	3SI3_NAJMO (Short neurotoxin 3) <i>Naja mossambica</i>
	16.4	LD ₅₀ : 0.45 μ g/mL	94.9 % (1:10) Response: 72.5 % (not diluted)	N.A.	N.A.	N.A.	No paralysis	6788.43	3S11_NAJPA (Short neurotoxin 1) <i>Naja pallida</i>
	16.4		76.9 % (1:10)					6788.43	3SA4_NAJHA (Cytotoxin 4) <i>Naja haje</i>
	16.4							6788.43	3SB2_HEMHA (Cytotoxin 2) <i>Hemachatus haemachatus</i>
	16.8	LD ₅₀ : 0.45 μ g/mL	Response: 90 % (not diluted)	N.A.	N.A.	N.A.	6 % paralysis	6832.46	3S11_NAJHA (short neurotoxin 1) <i>Naja haje</i>
	16.8		85.7 % (1:10)					6832.46	3SBH_HEMHA (Three-finger hemachatoxin) <i>Hemachatus haemachatus</i>
	16.8							6832.46	3SB1_HEMHA (Cytotoxin 1) <i>Hemachatus haemachatus</i>
	18.0	LD ₅₀ : 0.04 μ g/mL	Response: 85.7 % (not diluted) 86.9 % (1:10)	N.A.	N.A.	N.A.	64 % paralysis	6795.35	3SA8_NAJHA (Cytotoxin 8) <i>Naja haje</i>

peptides in the tryptic digests subsequently. Both the analytical column and the trapping column were placed in a column oven, of which the temperature was set at 45°C. The column eluate was transferred to the Bruker TIMS-TOF Mass Spectrometer, equipped with a captive spray ionisation (CSI) source in positive ion mode, for which the parameters of the CSI source were: source temperature, 150°C; desolvation temperature, 180°C; capillary voltage, 1300 V; gas flow, 3 L/min. The monitored mass range was m/z 300-3000 with a data-sampling time of 0.5 sec. The collision energy was 10 eV with prepulse storage of 10 μ s.

The raw MS/MS data from the nanoLC-ESI-MS/MS analyses were extracted using Bruker Data Analysis 5.0 and converted into deconvoluted extracted ion chromatograms (XICs). These deconvoluted XICs were then converted into Mascot generic format (MGF) files using Data Analysis 5.0. The resulting MGF files were uploaded to Mascot for database searches against two different databases: the Swiss-Prot database and a species-specific database for each respective venom. The

parameters used in the Mascot searches are explained as follows. The following parameters were used to achieve optimal results: (1) since iodoacetamide was used as an alkylating agent, the fixed modification: carbamidomethyl (C) was chosen (adding 34 Da to methionine amino acids); (2) the variable modifications: amidated (C-term) and methionine oxidation (M), (3) peptide tolerance of $\pm 0.1\%$ and MS/MS tolerance of ± 0.05 Da, (4) peptide charges of +1, +2, and +3.

2.6. Animal Care and Handling

All experiments complied with guidelines and regulations concerning the use of experimental animals, i.e. European Union (EU) directive no. 2010/63/EU and its implementation in The Netherlands: Wet op de Dierproeven. Zebrafish strain ABTL was kept at 28 °C in tanks with day/night light cycles of 10 h dark alternated with a 14 h light period. The zebrafish were handled in compliance with The Netherlands animal care

Table 2

Overview of tentatively assigned venom toxins associated with observed neurotoxicity (*in vitro* and/or *in vivo*). The table shows *m/z* values including the charge state corresponding to each *m/z*-value, retention times of plotted XICs, and the calculated accurate masses of the presented toxins. Proteomics data (from Mascot / Swiss-Prot database searches) for toxin identification and from there retrieved Mascot-derived exact masses are also given. Proteomics data was obtained by database searches of nanoLC-MS/MS data measured from tryptic digests of the respective venom toxins after nanofractionation and collecting these venom toxins from their respective wells in which they were fractionated.

Species	R. Time (min)	<i>m/z</i>	Charge	Accurate Mol. Mass (Da)	Protein Identification/Mascot Hits	Mascot Exact Mass (Da)	Toxin Class	
<i>Dendroaspis polylepis</i>	13.8	1145.95	7+	8010.61	3L21_NAJOX (Alpha-elapitoxin-Nno2a) <i>Naja oxiana</i>	8015.65	3FTx	
	14.6	1019.93	7+	7129.47	VKTA_MICTN (Kunitz-type neurotoxin MitTx-alpha) <i>Micrurus tener</i>	7120.99	KUN	
	15.0	938.04	7+	6555.23	VKTHK_DENPO (Kunitz-type serine protease inhibitor homolog dendrotoxin K (Fragment)) <i>Dendroaspis polylepis</i>	6555.31	KUN	
	15.2	937.27	7+	6549.83	3SX1_DENPO (Mambalglin-1) <i>Dendroaspis polylepis</i>	6549.96	3FTx	
	15.6	1007.31	7+	7040.16	3L24_DENPO (Alpha-elapitoxin-Dpp2d) <i>Dendroaspis polylepis</i>	7036.23	3FTx	
	15.8	1067.48	6+	6394.86	VKT2_WALAE (Kunitz-type serine protease inhibitor spermatin) <i>Walterinnesia aegyptia</i>	6394.25	KUN	
	16.0	1006.02	7+	7031.14	3SLS_DENPO (Calciseptin) <i>Dendroaspis polylepis</i>	7031.26	3FTx	
	16.2	1068.13	8+	8532.97	N.A.	N.A.	N.A.	
	16.4	999.34	8+	7982.68	3L24_DENPO (Alpha-elapitoxin-Dpp2d) <i>Dendroaspis polylepis</i>	7986.68	3FTx	
	16.8	1055.34	7+	7377.36	3SIM3_DENAN (Muscarinic toxin 3) <i>Dendroaspis angusticeps</i>	7376.45	3FTx	
	17.2	1083.32	7+	7572.17	3NO28_NAJNA (Weak neurotoxin 8) <i>Naja naja</i>	7570.90	3FTx	
	17.8	1081.83	6+	6481.97	VKT4_PSETT (Kunitz-type serine protease inhibitor textilin) <i>Pseudonaja textilis</i>	6490.93	KUN	
	18.2	415.19	20+	8284.96	N.A.	N.A.	N.A.	
	<i>Naja pallida</i>	13.5	1132.35	6+	6785.09	3SA7_NAJSP (Cytotoxin 7 Fragment) <i>Naja sputatrix</i>	6784.34	3FTx
		15.2	987.35	7+	6901.42	3S14_NAJHA (Short neurotoxin 4) <i>Naja annulifera</i>	6900.32	3FTx
		16.2	1027.17	7+	7178.15	N.A.	N.A.	N.A.
		16.6	963.19	7+	6732.29	3SA3_NAJKA (Cytotoxin 3) <i>Naja naja</i>	6731.85	3FTx
17.2		970.34	7+	6782.32	3S11_NAJPA (Short neurotoxin 1) <i>Naja pallida</i>	6782.10	3FTx	
17.4		982.34	7+	6865.35	3S11_NAJPH (Short neurotoxin 1) <i>Naja philippinensis</i>	6864.77	3FTx	
17.4		994.06	7+	6948.36	3S1CB_NAJNA (Cobrotoxin homolog) <i>Naja naja</i>	6943.98	3FTx	
17.4		984.77	7+	6883.39	3SA3_NAJMO (Cytotoxin 3) <i>Naja mossambica</i>	6881.42	3FTx	
17.8		1140.05	6+	6831.29	3S11_NAJHH (Short neurotoxin 1) <i>Naja haje</i>	6831.10	3FTx	
18.8		975.05	7+	6815.31	3SA1_NAJPA (Cytotoxin 1) <i>Naja pallida</i>	6814.31	3FTx	
<i>Hemachatus haemachatus</i>		11.6	975.87	7+	6821.04	3S1CC_NAJAT (Cobrotoxin-b) <i>Naja atra</i>	6821.05	3FTx
	13.2	978.58	7+	6840.06	3SIA4_NAJSP (Alpha-neurotoxin NTX-4) <i>Naja sputatrix</i>	6841.03	3FTx	
	15.4	1031.22	7+	7091.10	3SUB_DENAN (Muscarinic toxin) <i>Dendroaspis angusticeps</i>	7092.35	3FTx	
	15.8	1031.22	7+	7208.50	3SI3_NAJMO (Short neurotoxin 3) <i>Naja mossambica</i>	7210.58	3FTx	
	16.4	971.21	7+	6788.43	3S11_NAJPA (Short neurotoxin 1) <i>Naja pallida</i>	6782.10	3FTx	
	16.4	971.21	7+	6788.43	3SA4_NAJHA (Cytotoxin 4) <i>Naja haje</i>	6789.37	3FTx	
	16.4	971.21	7+	6788.43	3SB2_HEMHA (Cytotoxin 2) <i>Hemachatus haemachatus</i>	6787.44	3FTx	
	16.8	977.5	7+	6832.46	3S11_NAJHA (short neurotoxin 1) <i>Naja haje</i>	6831.05	3FTx	
	16.8	977.5	7+	6832.46	3SBH_HEMHA (Three-finger hemachatoxin) <i>Hemachatus haemachatus</i>	6831.45	3FTx	
	16.8	977.5	7+	6832.46	3SB1_HEMHA (Cytotoxin 1) <i>Hemachatus haemachatus</i>	6831.45	3FTx	
	18.0	972.34	7+	6795.35	3SA8_NAJHA (Cytotoxin 8) <i>Naja haje</i>	6799.32	3FTx	
	18.2	969.91	7+	6779.36	3SB3_HEMHA (Cytotoxin 3) <i>Hemachatus haemachatus</i>	6780.32	3FTx	
	19.2	973.06	7+	6801.34	3SAT_NAJAT (Cytotoxin 5) <i>Naja atra</i>	6802.37	3FTxt	

regulation and standard operating procedures. Zebrafish eggs were harvested at two hours post-fertilization (hpf), followed by incubation at 28 °C in egg water (sea salt, 60 µg/mL in tap water). The developing embryos were kept in an incubator at 28 °C. The breeding of adult zebrafish was conducted in a licenced establishment for the breeding and use of experimental animals (Leiden University) and was subject also to internal regulations and guidelines, with advice taken from the animal welfare body to minimise suffering for all experimental animals. The larvae used in these experiments had not reached the stage of exogenous (heterotrophic) feeding where the yolk sac had been exhausted (≤ 5 days post fertilisation (dpf)). Therefore, the experiments reported here are not considered animal experiments under the EU directive and Dutch law mentioned above, and so, a licence for working with these zebrafish larvae was not required.

2.7. Zebrafish Acute Toxicity Assay

To explore the toxins responsible for toxicity effects, we applied the approach consisting of RP-HPLC-nanofractionation of venoms (50 µL injection at 5 mg/mL concentration) into 96-well plates with a serpentine fashion fraction collection. Venom was separated using HPLC, followed by a post-column split in a 1:9 ratio, of which the smaller portion

went to UV and MS detection. The larger 90% portion went to the nanofractionation module, enabling high-resolution eluate collection. The eluate was then vacuum centrifuged to dryness overnight in a vacuum-centrifuge with a well plate rotor, then reconstituted with zebrafish embryo media and further diluted until the desired assay concentrations. For this, the dried venom toxins in each well plate were reconstituted in 250 µL medium and then diluted to another well plate in the following manner:

In the assay, the 5-fold geometric series were used. From these experiments, the highest concentrations of fractionated venom toxins (which can be translated to the highest venom concentrations which can be injected for each venom) for which none caused significant morbidity to the zebrafish venom can be assessed. For this experimental venom concentration range-finding, the geometric series of 5 dilutions, namely control (i.e., medium), 1x (stock/without dilution), 5x dilution, 25x dilution, and 125x dilution using embryo medium, were tested. A total of 50 microliters of reconstituted venom (assuming each well contains about 1 µg/mL of venom protein) is transferred to a new 96-well plate. Then, the dilution is performed in stages with the ratio of each 1:5, thus obtaining a series of concentrations of 1 (without diluting); 0.2; 0.04; 0.008 µg/mL. These diluted venom fractions (50 µL) were introduced to each corresponding well, which already has a single embryo and 50 µL

medium, giving the total volume per well 100 μ L. The protocol was carried out in three replicates. Embryos were generated by natural pairwise mating. Twenty pairs of adult zebrafish were set up for each mating, and, on average, 100-150 embryos per pair were generated. Embryos are maintained at 28 °C in embryo media. Embryos were cleaned (dead embryos were removed) and sorted by the developmental stage at 1-2 dpf. The 4 dpf developed zebrafish embryos were placed into wells containing embryo media and diluted venom using a micropipette one by one. The zebrafish embryos then were incubated for 24 hours in time to allow absorption of the venom toxins. The 5 dpf zebrafish embryos were then examined and scored manually by inspecting each embryo.

For the acute toxicity screening, 96-well microtiter plates were used. First, all outer wells were filled with water (100 μ L/well) instead of medium with a zebrafish embryo to prevent evaporation. The faster evaporation rate occurring on the outer wells of a well plate can namely influence the experiment's outcome and cause changes in compound concentration in these wells, caused by the so-called edge effect. In each well, 50 μ L embryo medium was transferred followed by one 4 dpf dechorionated zebrafish embryo.

The zebrafish toxicity assay was recorded at 4 dpf and again after 24 hours (5 dpf). The following criteria should be met for the embryo to be scored as 'dead': (1) tissue was opaque (milky-white) in appearance instead of transparent, (2) the heart was not beating, and (3) motionless (no locomotor activity). Each viable embryo will receive a score of 1, and each deceased embryo will receive a score of 0. The scoring was done by hand while looking through a microscope. Using the data from the acute toxicity assay, we determined the LD₅₀ values of all the fractionated venom toxins. The LD₅₀ values were calculated using the scored zebrafish embryo at 5 dpf. The statistical analysis using probit analysis enabled the extrapolation of the level of lethality of all fractionated venom toxins under *in vivo* conditions. The probit analysis function of the statistics program RTM and the complementary program RStudioTM, were used to calculate the LD₅₀ value for each venom fractions. The logarithmic function that resulted from extrapolating the scored dead embryo and the concentration that killed the embryo was obtained using the probit analysis tool. Consequently, the function can be used to determine the LD₅₀ values. These LD₅₀ values together with standard deviation for each fraction were plotted into so-called *in vivo* lethality chromatograms by plotting fractionation time on the X-axis vs LD₅₀ value with standard deviation in logarithmic scale on the Y-axis.

2.8. Cell Culture

Cell culture reagents were from Life Technologies Corporation, CA, USA, unless otherwise stated. The human neuroblastoma cell line SH-SY5Y was cultured in Roswell Park Memorial Institute (RPMI) medium supplemented with 15% FBS and 2 mM L-glutamine. Cells were maintained at 37 °C in a humidified 5% CO₂ incubator and subcultured every 3-4 days in a ratio of 1:5 using 0.25% trypsin/EDTA.

2.9. Nicotinic Acetylcholine Receptor $\alpha 7$ Calcium Influx Assay

Venom fractions were screened against $\alpha 7$ nAChR in SH-SY5Y cells using a Fluorescent Imaging Plate Reader (FLIPR Tetra; Molecular Devices, CA, USA) as previously described. Briefly, SH-SY5Y cells were plated at 40,000 cells per well in 384-well flat clear-bottom black plates (Corning, NY, USA) and cultured at 37 °C in a humidified 5% CO₂ incubator for 48 h before commencing assays. Cells were loaded with 20 μ L per well of Calcium 4 dye (Molecular Devices) reconstituted in assay buffer containing (in mM) 140 NaCl, 11.5 glucose, 5.9 KCl, 1.4 MgCl₂, 1.2 NaH₂PO₄, 5 NaHCO₃, 1.8 CaCl₂ and 10 HEPES pH 7.4, and containing the $\alpha 7$ agonist N-(5-chloro-2,4-dimethoxyphenyl)-N'(5-methyl-3-isoxazolyl)-urea (PNU120596) at 20 μ M final concentration, and plates incubated for 30 min at 37°C in a humidified 5% CO₂ incubator. Fluorescence responses were recorded at an excitation wavelength of 470-495 nm and emission of 515-575 nm for 10 s to set the baseline,

600 s after adding 1 μ g/mL fractionated venom toxin (from each well of the well plates containing fractionated toxins), and for a further 300 s after addition of 30 μ M choline. Tubocurarine at 50 μ M was used as $\alpha 7$ antagonist control.

2.10. L-Type CaV1.3 Calcium Influx Assay

Venom fractions were screened against CaV1.3 in SH-SY5Y cells using a Fluorescent Imaging Plate Reader (FLIPR Tetra; Molecular Devices, CA, USA) as previously described (1). Briefly, SH-SY5Y cells were plated at 40,000 cells per well in 384-well flat clear-bottom black plates (Corning, NY, USA) and cultured at 37 °C in a humidified 5% CO₂ incubator for 48 h before commencing assays. Cells were loaded with 20 μ L per well of Calcium 4 dye (Molecular Devices) reconstituted in assay buffer containing the CaV2.2 blocker CVIF at 1 μ M (Alomone Labs, Jerusalem, IL), and plates incubated for 30 min at 37°C in a humidified 5% CO₂ incubator. Fluorescence responses were recorded at excitation wavelengths of 470-495 nm and emission 515-575 nm for 10 s to set the baseline, 600 s after the addition of venom fractions, and 300 s after the addition of 90 mM KCl and 5 mM CaCl₂. Nifedipine at 10 μ M was used as CaV1.3 antagonist control.

2.11. Cytotoxicity Assay

Venom fractions were evaluated for lytic cytotoxic activity in SH-SY5Y cells using a Fluorescent Imaging Plate Reader (FLIPR Tetra; Molecular Devices, CA, USA) as previously described (Kramer et al 2024). Briefly, SH-SY5Y cells were plated at 40,000 cells per well in 384-well flat clear-bottom black plates (Corning, NY, USA) and cultured at 37 °C in a humidified 5% CO₂ incubator for 48 h before commencing assays. Cells were loaded with 20 μ L per well of Calcium 4 dye (Molecular Devices) reconstituted in assay buffer containing 50 μ M propidium iodide, and plates were incubated for 30 min at 37 °C in a humidified 5% CO₂ incubator. Fluorescence responses were recorded at excitation wavelengths of 470-495 nm and emission of 515-575 nm for intracellular calcium measurements and at excitation wavelengths of 470-495 nm and emission of 565-625 nm for DNA exposure measurements. Cells were recorded for 10 seconds to set the baseline and for 600 seconds after the addition of venom fractions. Triton X-100 at 0.025% was used as cytotoxicity control.

2.12. Zebrafish Paralysis Assay

For the zebrafish paralysis assay, 48-well microtiter plates were used. In each well, 200 μ L embryo medium was added, and 5 dpf dechorionated zebrafish embryos were then placed into the wells, 1 embryo per well. Then, 50 μ L of venom fraction solutions dissolved in embryo medium were added to the wells. The well plate was then introduced to the EthoVisionTM reader and examined for 50 min (10 min acclimatisation, 40 min for experiment) at 28 °C. The actual video recording started after 10 min of acclimatisation. The light and dark cycle was then introduced to the zebrafish embryos (the embryo will behave more actively during the dark phases compared to the light phases). Light and dark tests were carried out promptly (0-10 min light phase, 10-15 min dark phase, 15-25 min light phase, 25-30 min dark phase, and 30-40 min light phase). Under normal conditions, the movement of the zebrafish embryos will gradually decline over time under each condition due to fatigue and/or adaptation to the environment. The movement of embryos was filmed using the EthoVisionTM system equipped with a water bath and infrared camera. The video, which recorded all 48-wells simultaneously, was recorded at 60 frames per second which is sufficient to resolve the direction, speed, and duration of the slow spontaneous movement of the zebrafish embryos. The videos with the data of each well were recorded by Infrared camera using EthoVisionTM software and further analysed using EthoVisionTM software.

For the data processing, the exported numerical data of motion of the

zebrafish was plotted in the following manner:

$$\text{Ratio} = \frac{\sum \text{movements trials}}{\sum \text{movements controls}} \quad (\text{Equation 1})$$

Ratio = the movement ratio between each tested well and control well

$$\sum \text{movements trails} = ((\text{the accumulated movement in two dark phases (10 – 15 min and 25 – 30 min) of each well containing nanofractionated toxins}))$$

$$\sum \text{movements controls} = ((\text{the average accumulated movement in two dark phases (10 – 15 min and 25 – 30 min) of seven control wells})).$$

Next, using this data, paralysis chromatograms were plotted with on the X-axis the chromatographic retention time (in minutes) against on the Y-axis the average movement. In addition, the exported numerical data of motion and directions of the zebrafish over time was also plotted into 3D graphs by an in-house developed script written in MATLAB software. The processed data from the script, is visualized as follows: the first dimension (i.e., the X-axis) represents the chromatographic retention time (min), the second dimension (i.e., the Y-axis) gives the zebrafish paralyzing assay observation time (min), and the third dimension (i.e., the Z-axis) presents the total movement of the zebrafish embryo (mm).

3. Results

This study combined post-column ion channel targeted *in vitro* and behavioural zebrafish *in vivo* research in parallel with mass spectrometry and proteomics assessment (see Fig. 1) to study toxins from crude venoms. Datasets from cellular assays producing inhibition and activation of ion channels and zebrafish embryo *in vivo* lethality and paralysis assays produced so-named lethality and paralysis bioassay chromatograms (Figs. 2-4 and S Figures 1-5). A generic overview of the proteomics results is given in S Figure 8.

To investigate the toxicity of venom fractions, venoms were separated using RP-HPLC, nanofractionated into 96-well plates, vacuum-dried, reconstituted in zebrafish embryo media, and diluted following a 5-fold geometric series. Zebrafish embryos at 4 days post-fertilization (dpf) were individually exposed to the venom fractions, incubated for 24 hours, and scored manually for survival based on defined criteria. Acute toxicity was assessed by recording embryo viability and calculating LD₅₀ values through probit analysis using RTM and RStudioTM, and the results were plotted as *in vivo* lethality chromatograms. This comprehensive approach allowed the evaluation of the venom fractions' lethal potency in a high-throughput *in vivo* zebrafish model (See S Figure 9).

For the zebrafish paralysis assay, 5 dpf dechorionated embryos were placed individually into 48-well plates, exposed to venom fractions, and their movements were recorded using the EthoVisionTM system under alternating light and dark phases. After a 10-minute acclimatisation, embryo movements were filmed for 40 minutes at 28 °C, and the data were analysed to assess paralysis effects. A typical phenotype observed in the zebrafish paralysis assay was reduced swimming activity, where

affected embryos displayed significantly decreased or absent spontaneous movement compared to healthy controls, despite maintaining heartbeat and general structural integrity.

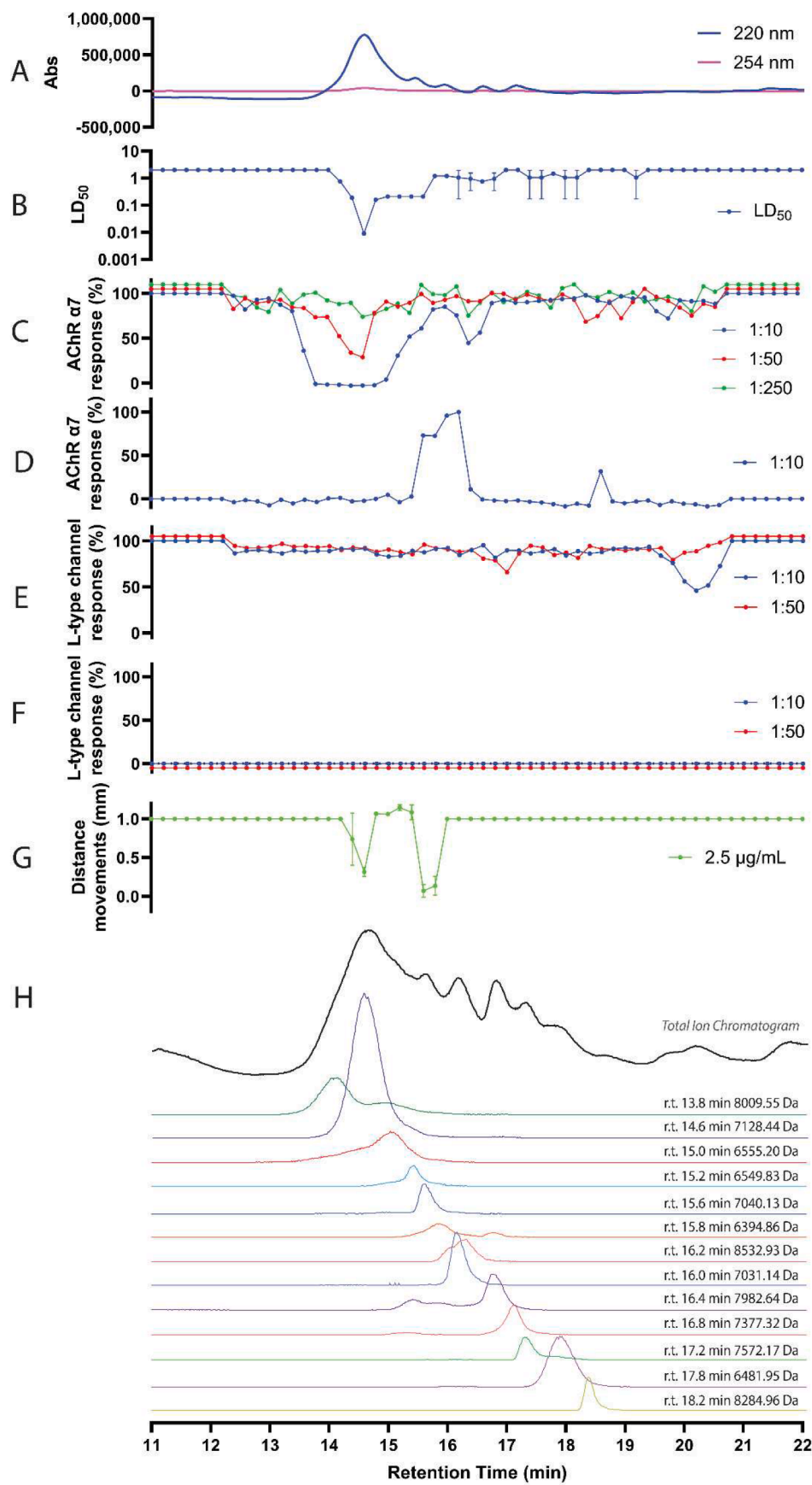
These were then superimposed and further correlated with LC-UV chromatograms and MS proteomic data to facilitate identification of the bioactive toxins. Of all venoms analysed, *D. polylepis* (Fig. 2), *N. pallida* (Fig. 3), and *H. haemachatus* (Fig. 4) venoms showed the most

interesting bioactivities due to strong correlation between ion channel activity and zebrafish paralysis, which was not observed consistently in other venoms, while results obtained from other less bioactive elapid

snake venoms (*Dendroaspis angusticeps*, S Figure 1; *Dendroaspis viridis*, S Figure 2; *Naja mossambica*, S Figure 3; *Naja haje*, S Figure 4; and *Naja naja*, S Figure 5) are presented in the Supporting Information. For *D. polylepis*, *N. pallida*, and *H. haemachatus* venoms, a comprehensive data summary of the chemical data acquired from the bioactive venom fractions, together with the biochemical and biological data, are provided in Table 1. For the other venoms analysed, this data is provided in the Supporting Information S Table 1. These tables report the retention times of the fractionated and post-column analysed toxins, the summarised *in vitro* and *in vivo* bioassay responses measured, and toxin accurate masses measured next to toxin identification results acquired from the proteomics data.

3.1. *Dendroaspis polylepis*

The integrated chromatographically represented data of the *D. polylepis* (Tanzania) venom analysis results are depicted in Fig. 2. All relevant processed numerical data from the combined datasets for *D. polylepis* venom are provided in Table 2. *D. polylepis* venom showed significant inhibition (50-100%) on the α7 nAChR ion channel. Particularly noteworthy, Fig. 2C displays an extensive negative peak of inhibition (13.0-16.0 min) of the α7 nAChR ion channel by *D. polylepis* venom toxins at the highest concentration tested. Eluting toxins in this time frame completely inhibited calcium influx in the bioassay. At a lower venom toxin concentration tested (shown as the red chromatogram in Fig. 2C), a negative peak was clearly visible around 14.5 min. Based on the LC-MS and proteomics data, toxins eluting at this time frame were three-finger toxins (3FTxs) and Kunitz-type serine protease inhibitors. There were six 3FTxs found in the relevant retention time frame of 13.0 – 16.0 min ranging from 6 kDa to 8 kDa (Fig. 2H; Table 2). Three toxins with masses of 8010.61 Da (14.0 min), 7129.47 Da (14.4 min), and 6555.23 Da (14.8 min) are suspected of acting as inhibitory agents of the α7 nAChR ion channel. Three toxins, with masses of 7040.16 Da (15.3 min), 8532.97 Da (15.8 min) and 7982.68 Da (16.4 min) are suspected of acting as activators of the α7 nAChR. The paralysis chromatogram (Fig. 2G) shows the retention times of 13.8 min and 15.6 min negative paralysis peaks indicating toxin-induced paralysis of the zebrafish. The paralysis peak at 14.6 min correlated with a protein-accurate mass of 7129.47 Da. The paralysis peak at 15.6 min correlated with a protein mass of 7040.16 Da observed in the *in vitro* α7



(caption on next page)

Fig. 2. Aligned traces of LC-UV and LC-MS chromatogram data with bioassay chromatogram data of analysed *D. polylepis* venom. (A) LC-UV chromatogram of *D. polylepis* venom (1 mg/mL, 50 μ L injection volume, post-column split into 1:9 ratio of which the smaller portion went to UV [220 and 254 nm recorded] and MS), and the larger portion to nanofractionation for subsequent bioassaying or proteomics; (B) LD₅₀ bioassay chromatogram. Five geometric series of venom dilution (performed in three replicates) and probit analysis was used to construct the LD₅₀ bioassay chromatogram; (C) Inhibition of the α 7 nicotinic acetylcholine receptor (α 7 nAChR) measured by a calcium influx assay; (D) activation of the α 7 nAChR measured by the calcium influx assay; (E) inhibition of the L-type channel measured by a calcium influx assay; (F) activation of the L-type channel measured by the calcium influx assay; (G) zebrafish paralysing assay chromatogram results; (H) MS extracted ion currents (XICs).

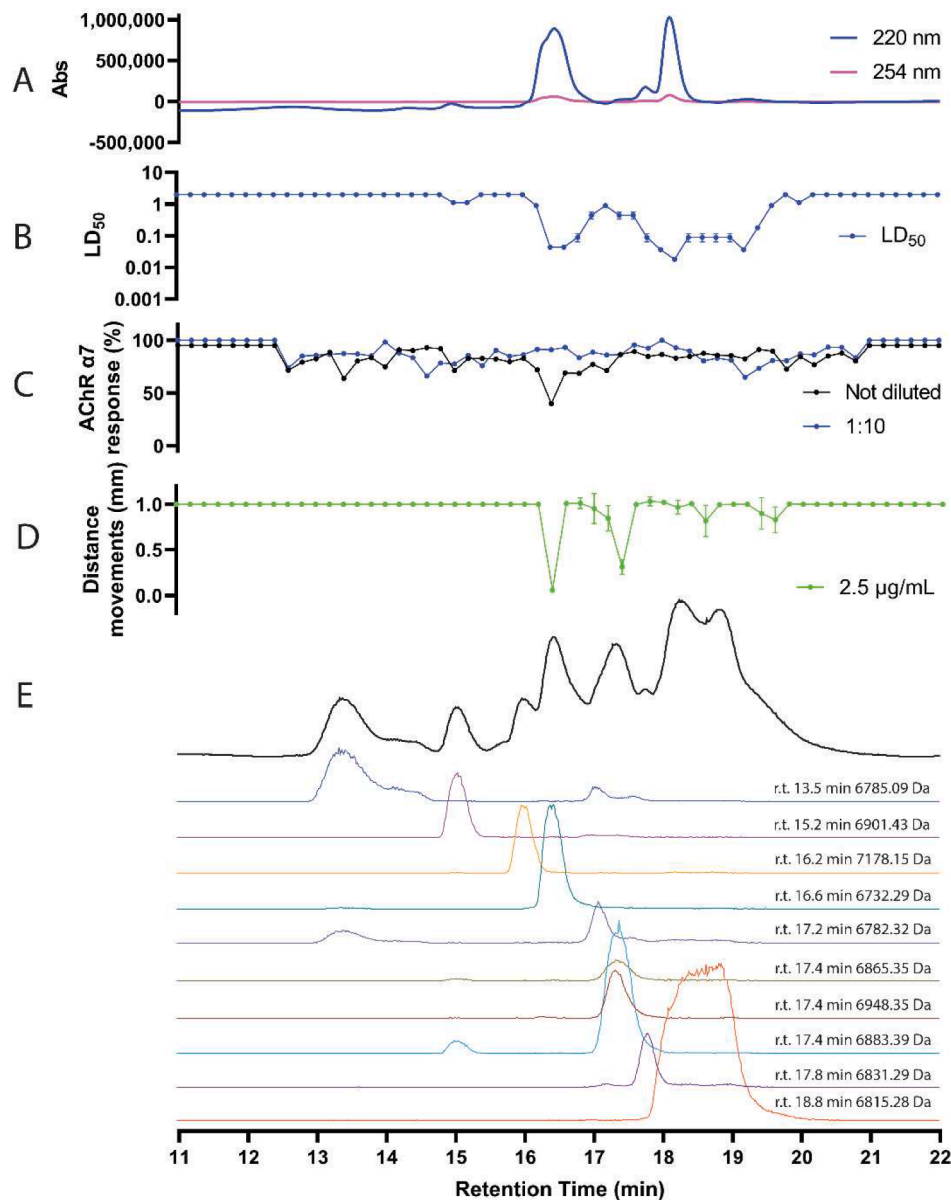


Fig. 3. Correlation of LC-UV and LC-MS data with bioassay chromatogram data of *N. pallida* venom. (A) LC-UV chromatogram of *N. pallida* venom; (B) LD₅₀ bioassay chromatogram. Five geometric series of venom dilution (performed in three replicates) and probit analysis were used to construct the LD₅₀ bioassay chromatogram; (C) Inhibition assay of the α 7 nicotinic acetylcholine receptor measured by a calcium influx assay; (D) zebrafish paralysing assay chromatogram results; (E) extracted ion currents (XICs) from the LC-MS data.

nAChR ion channel activation bioassay signals. Mascot searches of tryptic digests of fractionated *D. polylepis* bioactive venom toxins resulted mainly in 3FTxs and some Kunitz-type serine protease inhibitors. The three-finger toxins α -elapitoxin-Dpp2d (15.6 min fraction; 3L24_DENPO; 7040.16 Da) and a Kunitz-type neurotoxin MitTX- α (14.6 min fraction; VKTA_MICTN; 7129.47 Da) were the predominant constituents found for the main bioactivity peaks. To summarize, the first paralysis peak correlated with the broad inhibitory α 7 nAChR peak,

which turned into a sharper matching peak after testing in the α 7 nAChR bioassay using diluted nanofractionated venom toxins. For this peak, in the LD₅₀ chromatogram data a clear negative peak was also observed showing lethality at this retention time. The responsible toxin(s) for the paralysis at high concentration thus resulted in the death of the zebrafish. The second paralysis peak matched with the α 7 nAChR activation peak. For the L-type ion channel, no bioactivity was observed in the bioassay for the *D. polylepis* venom (see Fig. 2E and 2F, and Table 2).

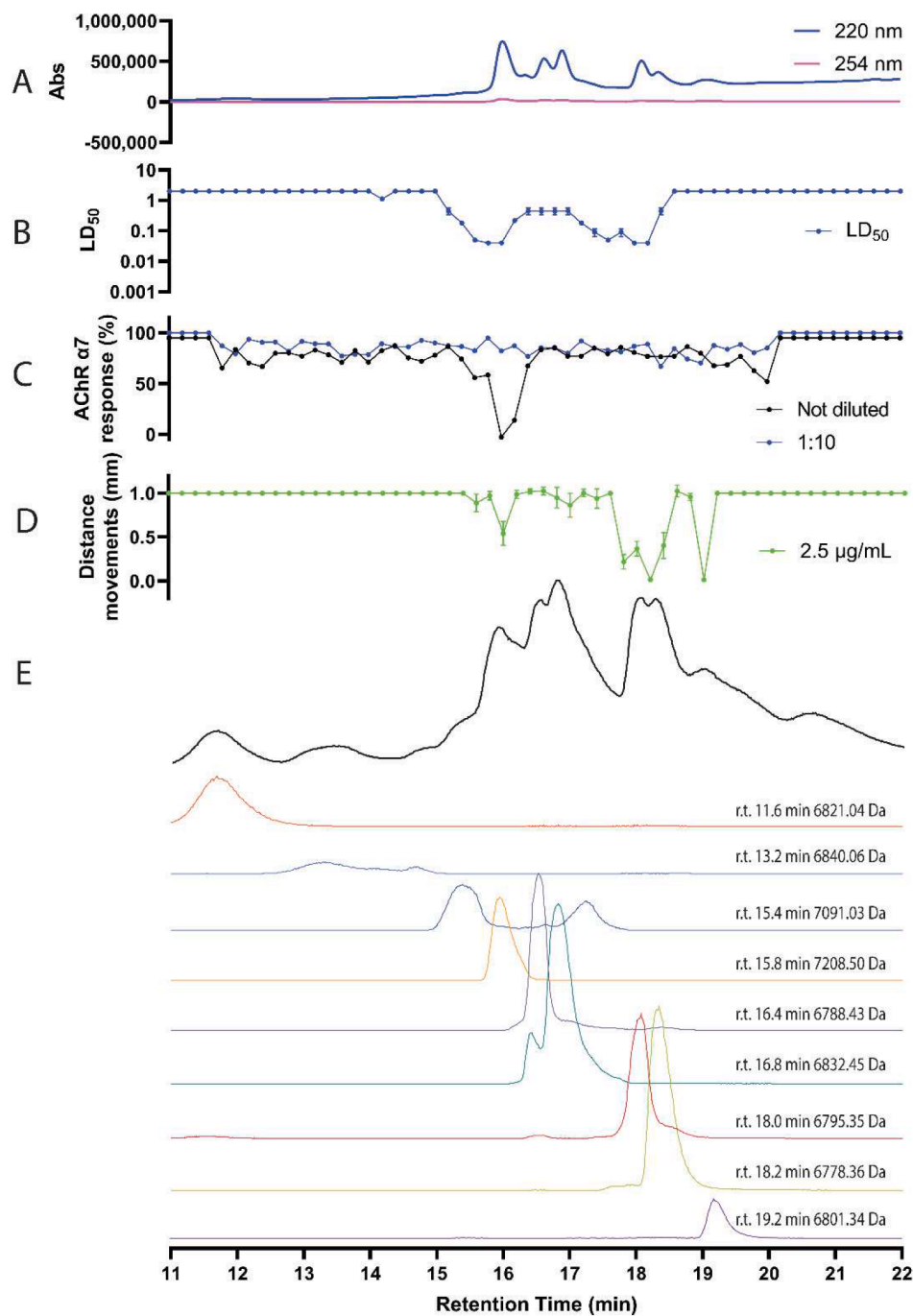


Fig. 4. Correlation of LC-UV and LC-MS data with bioassay chromatogram data of *H. haemachatus* venom. (A) LC-UV chromatogram of *H. haemachatus* venom; (B) LD₅₀ bioassay chromatogram. Five geometric series of venom dilution (performed in three replicates) and probit analysis was used to construct the LD₅₀ bioassay chromatogram; (C) Inhibition of $\alpha 7$ nicotinic acetylcholine receptor measured by a calcium influx assay; (D) zebrafish paralyzing assay chromatogram; (E) extracted ion currents (XICs) from the LC-MS data.

3.2. *Naja pallida*

Fig. 3 shows the results of *N. pallida* (Tanzania) venom analysis. All relevant processed data from the combined datasets for *N. pallida* venom is shown in Table 1. The LD₅₀ chromatogram for the *N. pallida* profile ranges in bioactivity profile in terms of negative peaks from 0.01 to 1.3 $\mu\text{g}/\text{mL}$, indicating severe toxicity with a high potency. The negative peaks showing lethality toxicity are seen at retention times 16.4, 18.0 and 19.0 min. According to the LC-MS data, within these time frames, masses within the mass ranges of 3FTxs and PLA₂s were mainly found. Table 2 presents the relevant masses found. At 16.4 min rt, there is a

protein with a mass of 6732.29 Da, which corresponds to the 3FTx mass range. Proteomics data at rt, 16.6 min yielded a main match with the protein 3SA3.NAJKA (cytotoxin 3; *Naja kaouthia*). For the proteins eluting at 17.8 and 18.8 min, no clear matching toxin accurate masses could be found from the LC-MS data. According to the proteomics data on the toxins eluting around these retention times, it was found that numerous toxins coeluted, particularly three-finger toxins and phospholipase A₂s (PLA₂s). Inhibition peak results in the $\alpha 7$ nAChR chromatogram showed a substantial negative peak at 16.6 min, matching with the paralysis peak found at the same retention time. The other negative peak in the paralysis chromatogram was at 17.4 min. This

negative peak showed a clearly observed toxin with a mass of 6883.39 Da, as deduced from the LC-MS data (see Table 2). From the proteomics data, at 17.4 min a main match was found with the protein 3SA3_N-AJMO (cytotoxin 3; *Naja mossambica*). To summarize, the first main peak showing paralysis in fact caused lethality to the zebrafish. No clear *in vitro* bioassay response was observed, although a small inhibitory peak was seen for the $\alpha 7$ nAChR inhibition, indicating other ion channels and/or receptors are likely involved in this observed *in vivo* activity and that warrants further investigation in future studies. The second paralysis peak was not correlated to lethality and also not to any of the ion channels tested in this study. For this paralysis peak, the responsible target thus remains unknown.

3.3. *Hemachatus haemachatus*

Fig. 4 shows the *H. haemachatus* (South Africa) venom analysis results. All relevant processed data from the combined datasets for *H. haemachatus* venom is shown in Table 1. The LD₅₀ chromatogram of *H. haemachatus* displays a range of negative bioactivity peaks from 0.1 to 1.3 $\mu\text{g}/\text{mL}$, indicating a lower toxicity level of *H. haemachatus* venom as compared to *D. polylepis* and *N. pallida* venoms. The LC-MS data showed that within the retention time profiles where the lethality toxicity-causing peaks eluted, the corresponding accurate masses found were in the mass ranges of 3FTxs and PLA₂s (see Table 2). The negative lethality peaks were found at retention times of 15.8, 18.0- and 18.2-min. Table 2 shows an accurate mass of 7208.50 Da for a main toxin found at 15.8 min, tentatively identified as a 3FTx. Proteomics data obtained within this retention period was used to tentatively identify the corresponding toxins for which 3SI3_NAJMO (short neurotoxin 3; *Naja mossambica*) was found as a main candidate. The paralysis bioactivity chromatogram displayed four distinct negative peaks for the *H. haemachatus* venom results. These negative peaks were observed at retention times of 15.8, 18.0, 18.2 and 19.2 min. The paralyzing chromatogram's largest negative peak at a retention time frame of 18.0 min to 18.2 min gave multiple closely co-eluting toxins, including acidic phospholipase A₂ 2 (PA2A2_NAJNA) and basic phospholipase A₂ 1 (PA2B1_HEMHA) found at the respective retention times from the proteomics data. A candidate toxin detected around 18.0 min from the LC-MS data was likely a 3FTx, with an accurate mass of 6795.35 Da. A main match from the proteomics data was 3SA8_NAJHA (Cytotoxin 8; from *Naja haje*). Due to the broad main peak in the paralyzing bioassay chromatogram, there were multiple toxins found that possibly contributed to the bioactivity observed at retention time 18.0-18.2 min including a toxin eluting at a retention time of 18.0 min corresponding to a toxin with an accurate mass of 6795.35, deduced from the LC-MS data as 3SA8_NAJHA (Cytotoxin 8; *Naja haje*). In Table 2, for the retention time of 18.2 min the toxin 3SB3_HEMHA (cytotoxin 3 from *Hemachatus haemachatus*) was found with an accurate mass of 6779.36 Da deduced from the LC-MS data. The $\alpha 7$ nAChR receptor inhibition results shown as bioassay chromatogram data in Fig. 4 C give a strong negative peak at 15.8 min, correlating to the first (broad) lethality-toxicity peak from the LD₅₀ data and a peak observed in the 'paralysis' chromatogram. The latter two major paralysis peaks could not be correlated to the *in vitro* tested ion channel and receptor targets implying that other molecular targets are responsible for the observed *in vivo* effects.

3.4. Other venoms analysed using the workflow

Venoms of the snakes *Dendroaspis angusticeps* (Tanzania), *Dendroaspis viridis* (Togo), *Naja mossambica* (Tanzania), *Naja naja* (captive bred), and *Naja haje* (Uganda) were also investigated in this study, combining *in vivo* and *in vitro* post-column bioassaying data with chemical toxin characterisation data. For these venoms, less clear correlations between *in vitro* and *in vivo* data, and accurate mass spectrometry and proteomics data, were found as compared to the venoms of *Dendroaspis polylepis*,

Naja pallida and *Hemachatus haemachatus*. A comprehensive data summary of the chemical data acquired from the bioactive venom fractions, together with the biochemical and biological data, is provided in Supporting Information, S Table 1. For the same venoms, Supporting Information, S Table 2 provides processed chemical mass spectrometry data for which the accurate mass data of the relevant toxins in detail (including *m/z*-values and charge states). The accompanying superimposed chromatographic results per venom are provided in the Supporting Information as Supplementary S Figures 1-5, showing *D. angusticeps*, *D. viridis*, *N. mossambica*, *N. haje* and *N. naja*, respectively.

3.5. Assay for potential cell lysis

As some venom toxins can act with cytotoxic lytic effects thereby potentially masking the desired bioassay readouts of the $\alpha 7$ nAChR and L-type calcium channel assays, we performed additional assays to further investigate whether potential cell lysis caused by venom toxin exposure. This was done using a multiplex bioassay using fluorescence imaging measuring simultaneously intracellular calcium responses and DNA release indicative of cell lysis in cells exposed to the venom toxins [36]. These tests revealed that the calcium responses induced by these venom toxins occurred in the absence of DNA release and therefore no cytotoxicity and no calcium release was observed in place for any of the *in vitro* assays performed during this study (S Figure 6 and S Figure 7).

4. Discussion

The purpose of this study was to establish a new analytical profiling technique for assessing post-column bioactivity profiling of *in vitro* and *in vivo* effects of elapid venom toxins in combination with toxin identifications. The methodology was demonstrated to examine the deleterious effect of elapid snake venom from the mamba (*Dendroaspis*) and cobra (*Naja*) and Rinkhals (*Hemachatus*) genera on molecular processes *in vitro* followed by *in vivo* effects on a living vertebrate model, the larval zebrafish (*Danio rerio*). It is known that elapid snake venoms comprise a complex mixture of proteins and peptides, including neurotoxins and cytotoxins, which can have diverse effects on various animal models. This work integrates post-column *in vitro* calcium influx assays investigating $\alpha 7$ nAChR and L-type calcium channels with behavioural *in vivo* research (i.e., lethality and paralyzing assays).

The Table 1-2 and S Table 1-2 present a comparative analysis of various venom fractions across multiple species, focusing on their chemical properties, *in vitro*, and *in vivo* bioassay responses, and protein identification. The LC₅₀ values spanned a broad range of 0.009 to 1.12 $\mu\text{g}/\text{mL}$, indicating different potencies. The primary assays tested were nAChR $\alpha 7$ receptor calcium influx (negative peaks), activator assays (positive peaks), L-type calcium channel assays, and paralyzing assays. Paralysis was observed particularly in fractions associated with proteins like calciceptin (3SLS_DENPO), Kunitz-type neurotoxin MitTx-alpha (VKTA_MICTN), alpha-elapitoxin-Dpp2d (3L24_DENPO), and alpha-elapitoxin-Nn2a (3S12_NAJNA). Several venom components, especially three-finger toxins, Kunitz-type protease inhibitors, and cytotoxins, were implicated in bioactivities such as neurotoxicity and muscle paralysis.

Our findings demonstrated that exposure of zebrafish larvae to the venoms of the elapid snakes produced significant *in vivo* effects. Venoms caused dose-dependent lethality, with higher venom concentration causing faster larval death. This clearly indicated that the venoms under study contained potent toxins that can induce acute toxicity in vertebrates. Toxicity screening on zebrafish embryos has become a routine procedure for determining and assessing the toxicity and mortality of toxic substances (see S Figure 9) [37,38].

Nanofractionation analytics has been applied to study various venom toxin bioactivities, including enzyme inhibition, and protease activities, highlighting its potential for drug discovery and biotechnology [34, 39-41]. Studies by Zietek et al. (2018), demonstrated its effectiveness in

profiling complex venom compositions and exploring therapeutic possibilities [41]. Furthermore, Otvos *et al.* (2016) expanded nanofractionation analytics to mammalian cellular bioassaying by using a calcium influx assay to screen for compounds targeting the $\alpha 7$ -nicotinic acetylcholine receptor, focusing on toad skin secretions [40]. These advancements show the broader application of nanofractionation methods to natural product discovery and biomedical research.

For acute toxin exposure, injections (which are often used in rodent models) and immersion are appropriate for the zebrafish model. We demonstrated successful post-column *in vivo* lethality profiling of elapid venom toxins. Because the venom toxins analysed in this study were exposed to the zebrafish embryos after analytical separation and were collected as adjacent fractions, and because the zebrafish toxin exposure (i.e., venom toxins dissolved in the swimming water in this study) differs from typical rodent exposure (i.e., often IV or IP injection), determining actual toxin doses tested is difficult.

In zebrafish larvae, venom components may enter the systemic circulation through several potential routes. Passive diffusion enables small, lipophilic molecules to transverse epithelial barriers without energy expenditure. Alternatively, receptor-modulated uptake may facilitate the internalisation of specific venom protein through interaction with cellular surface receptors, leading to active transport process. Epithelial absorption, particularly across the integumentary or mucosal surfaces, also represents a critical pathway for allowing diverse venom constituents to permeate biological membranes and exert systemic effects.

The zebrafish larval model's strength resides in its high-throughput nature by means of well-defined behavioural patterns. In our results, ion channels that mediate behaviour and/or locomotion can be studied *in vitro* alongside the zebrafish *in vivo* responses to the corresponding toxins. Despite obvious differences between zebrafish and humans, the zebrafish has characteristics that complement the mammalian models often used in behavioural sciences [42]. In terms of the genome, brain patterning, and the structure and functioning of various neurological and physiological systems, zebrafish share extensive homologies with other vertebrate species. Because of their swimming ability and the functionality of their motor, sensory, and stress-regulating systems, zebrafish embryos represent a valuable model for early-stage behavioural testing.

Despite the promising results, this study has several limitations. Firstly, the complexity of elapid venoms, which contain a diverse array of proteins and peptides, poses challenges in isolating and identifying individual toxins responsible for specific bioactivities. The post-column separation method, while effective, may not fully resolve all venom components, potentially leading to the presence of overlapping fractions.

Additionally, the exposure method used in zebrafish larvae (dissolved in swimming water) differs significantly from the intravenous or intraperitoneal injections commonly used in rodent models, complicating direct comparisons of venom potency and effects across species.

Furthermore, the zebrafish model, while advantageous for high-throughput screening, may not fully replicate the physiological responses observed in mammals, limiting the extrapolation of findings to human health.

It is plausible that the observed effects on zebrafish larvae are mediated by venom components targeting multiple ion channels and physiological systems. In addition to direct modulation of voltage-gated channels, toxins may interfere with muscarinic receptors, GABAergic signalling pathways, or cardiovascular function, collectively contributing to the locomotor and paralytic deficits observed. Notably, no major developmental malformations were detected during the study period, suggesting that the primary manifestations of venom exposure are functional rather than structural, with a particular emphasis on impaired mobility and paralysis.

Future research should aim to refine the separation and identification techniques to achieve more precise fractionation of venom

components, potentially employing advanced chromatographic and mass spectrometric methods. Expanding the study to include additional *in vitro* assays targeting other ion channels and receptors could provide a more comprehensive understanding of the venom's molecular mechanisms.

The findings of this study highlight that bioactivity, as reflected by locomotor and paralytic outcomes, does not always correlate directly with the extent of ion channel inhibition observed *in vitro*. This discrepancy suggests the involvement of additional molecular targets or complex physiological interactions that are not solely dependent on ion channels blockade. Therefore, further mechanistic studies are necessary to elucidate the specific pathways and targets responsible for the observed bioactivity.

Investigating the potential therapeutic applications of identified venom toxins, particularly those with specific ion channel modulatory effects, could lead to the development of novel pharmacological agents. Finally, integrating omics technologies, such as transcriptomics and proteomics, could offer deeper insights into the systemic responses elicited by venom exposure, paving the way for more targeted and effective antivenom strategies.

The relevance of venom-targeted ion channels to human physiology underscores the translational potential of this research. Insights gained from venom bioactivity may aid in the identification of novel therapeutic targets and facilitate the development of lead compounds for the treatment of envenomation. Moreover, the integrated screening pipeline established in this study provides a valuable platform for accelerating early-stage drug discovery efforts aimed at modulating ion channels functioning.

5. Conclusion

In this study, we have integrated three key parameters of venom toxicity: (i) the chemical identification of the active toxins, (ii) the *in vitro* ion channel modulation by toxin fractions, and (iii) their *in vivo* toxicity including their paralyzing effects. We have used automated video tracking further to complement the observations on zebrafish larvae' behaviour patterns. We used video-tracking software to generate additional endpoints such as distance travel, and swimming behaviour (in 48-well plate format) in the form of swimming vectors and trails. The study provided complex high-content data displayed in multiple datasets in parallel. Included in the display are LC-UV, LC-MS TICs and XICs, LD₅₀s, ion channel functioning, and paralyzing readouts for toxins from venoms of the mamba and cobra genus under investigation. When these multiple data readouts are superimposed, venom fraction relative abundances could be deduced from LC-UV, their toxin masses from the LC-MS data, toxin IDs could be retrieved from the additional proteomics analyses. Most importantly, these chemical analyses could be correlated with the targeted *in vitro* ion channel bioassay chromatograms and the *in vivo* lethality and behavioural chromatograms which were constructed by plotting the fractionation time of toxins over behavioural responses.

Lead Contact

Further information and request for resources should be directed to and will be fulfilled by the lead contact Jeroen Kool (j.kool@vu.nl).

Data availability statement

Data is available upon request.

Statements and Declarations

Funding

This research was funded by an Indonesian Endowment Fund for Education (LPDP) Ph.D. research studentship [S-5622/LPDP.4/2020] to

A.A.

Institutional Review Board Statement

Not applicable.

Informed Consent Statement

Not applicable.

CRediT authorship contribution statement

Arif Arrahman: Writing – original draft, Visualization, Validation, Software, Resources, Project administration, Methodology, Investigation, Funding acquisition, Formal analysis, Data curation. **Haifeng Xu:** Formal analysis, Data curation. **Muzaffar A. Khan:** Formal analysis, Data curation. **Tijmen S. Bos:** Software, Data curation. **Julien Slagboom:** Software, Methodology, Formal analysis, Data curation. **Guus C. van der Velden:** Methodology, Formal analysis. **Ulrike Nehrlich:** Data curation. **Nicholas R. Casewell:** Writing – review & editing, Resources. **Michael K. Richardson:** Writing – review & editing, Supervision, Resources. **Christian Tudorache:** Writing – review & editing, Validation, Supervision, Resources, Methodology, Formal analysis, Data curation. **Fernanda C. Cardoso:** Writing – review & editing, Visualization, Validation, Software, Resources, Project administration, Methodology, Investigation, Formal analysis, Data curation. **Jeroen Kool:** Writing – review & editing, Writing – original draft, Visualization, Supervision, Software, Resources, Methodology, Investigation, Formal analysis, Conceptualization.

Declaration of competing interest

None of the authors (Arif Arrahman, Haifeng Xu, Muzaffar A. Khan, Tijmen S. Bos, Julien Slagboom, Guus C. van der Velden, Ulrike Nehrlich, Nicholas R. Casewell, Michael K. Richardson, Christian Tudorache, Fernanda C. Cardoso, and Jeroen Kool) declare a competing interest.

Acknowledgments

The authors thank Paul Rowley and Edouard Crittenden for the maintenance of snakes at the LSTM and for the provision of venoms.

Supplementary materials

Supplementary material associated with this article can be found, in the online version, at [doi:10.1016/j.slasd.2025.100239](https://doi.org/10.1016/j.slasd.2025.100239).

Supplemental Information: S Figure 1. Correlation of LC-UV and LC-MS chromatogram data with bioassay chromatogram data of analysed *Dendroaspis angusticeps* venom. **S Figure 2.** Correlation of LC-UV and LC-MS chromatogram data with bioassay chromatogram data of analysed *Dendroaspis viridis* venom. **S Figure 3.** Correlation of LC-UV and LC-MS chromatogram data with bioassay chromatogram data of analysed *Naja mossambica* venom. **S Figure 4.** Correlation of LC-UV data and LC-MS chromatogram data with bioassay chromatogram data of analysed *Naja haje* venom. **S Figure 5.** Correlation of LC-UV data and LC-MS chromatogram data with bioassay chromatogram data of analysed *Naja naja* venom. **S Figure 6.** Evaluation for lytic cytotoxic activity in SH-SY5Y cells using a Fluorescent Imaging Plate Reader (FLIPR) of *D. Polylepis*, *D. angusticeps*, *D. viridis*, *N. naja*, *N. mossambica*, *N. haje*, *N. pallida*, and *H. haemachatus* venoms at different concentrations. **S Figure 7.** Evaluation for lytic cytotoxic activity in SH-SY5Y cells using a Fluorescent Imaging Plate Reader (FLIPR) of *D. Polylepis*, *D. angusticeps*, *D. viridis*, *N. naja*, *N. mossambica*, *N. haje*, *N. pallida*, and *H. haemachatus* venoms at different concentrations. **S Figure 8.** Global overview of proteomics searches using Mascot against the Swiss-Prot database to identify venom toxins of *D. Polylepis*, *D. angusticeps*, *D. viridis*, *N. naja*, *N.*

mossambica, *N. haje*, *N. pallida*, and *H. haemachatus* venoms. **S Figure 9.** Schematic overview of analytical platforms used for *in vivo* bioassaying with zebrafish embryos. **S Table 1.** Overview of analysed venoms and bioactivity peaks. **S Table 2.** Overview of tentatively assigned venom toxins associated with observed neurotoxicity (*in vitro* and/or *in vivo*). The table shows *m/z* values including the charge state corresponding to each *m/z*-value, retention times of plotted XICs, and the calculated accurate masses of the presented toxins.

References

- [1] William KH, Shelton SH, Curtis GR, Joseph FG. *Biol. Vipers* 2002;207–33.
- [2] Kazandjian TD, Petras D, Robinson SD, van Thiel J, Greene HW, Arbuckle K, Barlow A, Carter DA, Wouters RM, Whiteley G, Wagstaff SC, Arias AS, Albuilescu LO, Plettenberg Laing A, Hall C, Heap A, Penrhyn-Lowe S, McCabe CV, Ainsworth S, da Silva RR, Dorrestein PC, Richardson MK, Gutiérrez JM, Calvete JJ, Harrison RA, Vetter I, Undheim EAB, Wüster W, Casewell NR. *Science* (80-) 2021; 371:386–90.
- [3] Bittenbinder MA, Zdenek CN, Op Den Brouw B, Youngman NJ, Dobson JS, Naude A, Vonk FJ, Fry BG. *Toxins* (Basel) 2018;10.
- [4] Ferraz CR, Arrahman A, Xie C, Casewell NR, Lewis RJ, Kool J, Cardoso FC. *Front. Ecol. Evol.* 2019;7:1–19.
- [5] Kini RM. *Acta Chim. Slov.* 2011;58:693–701.
- [6] Pawlak J, Kini RM. *Biochimie* 2008;90:868–77.
- [7] Rahman MM, Teng J, Worrell BT, Noviello CM, Lee M, Karlin A, Stowell MHB, Hibbs RE. *Neuron* 2020;106:952–962.e5.
- [8] Xie C, Bittenbinder MA, Slagboom J, Arrahman A, Kool J. *J. Chromatogr. B* 2021; 122586.
- [9] Slagboom J, Kool J, Harrison RA, Casewell NR. *Br. J. Haematol.* 2017;177:947–59.
- [10] Jamunaa A, Vejjayan J, Halijah I, Sharifah SH, Ambu S. *J. Venom. Anim. Toxins Incl. Trop. Dis.* 2012;18:150–6.
- [11] Muñoz LM, Holgado BL, Martínez-A C, Rodríguez-Frade JM, Mellado M. *Immunol. Lett.* 2012;145:23–9.
- [12] Servent D, Blanchet G, Mourier G, Marquer C, Marcon E, Fruchart-Gaillard C. *Toxicol* 2011;58:455–63.
- [13] Spies M, Lips KS, Kurzen H, Kummer W, Haberberger RV. *J. Mol. Neurosci.* 2006; 30:55–6.
- [14] Ferraz CR, Arrahman A, Xie C, Casewell NR, Lewis RJ, Kool J. *F.C. Cardoso, Front. Ecol. Evol.* 2019;7.
- [15] Kini RM, Doley R. *Toxicol* 2010;56:855–67.
- [16] Silva A, Hodgson WC, Isbister GK. *Toxins* (Basel) 2017;9:1–17.
- [17] Faiz MA, Ghose A, Ahsan MF, Rahman MR, Amin MR, Hassan MMU, Chowdhury MAW, Kuch U, Rocha T, Harris JB, Theakston RDG, Warrell DA. *Brain* 2010;133:3181–93.
- [18] Gonçalves TC, Benoit E, Kurz M, Lucarain L, Fouconnier S, Combemale S, Jaquillard L, Schombert B, Chambard JM, Boukaiba R, Hessler G, Bohme A, Bialy L, Hourcade S, Bérout R, De Waard M, Servent D, Partiseti M. *Br. J. Pharmacol.* 2019; 176:1298–314.
- [19] Gonçalves TC, Benoit E, Partiseti M, Servent D. *Front. Pharmacol.* 2018;9.
- [20] Cardoso FC, Pineda SS, Herzig V, Sunagar K, Shaikh NY, Jin AH, King GF, Alewood PF, Lewis RJ, Dutertre S. *Int. J. Mol. Sci.* 2022;23.
- [21] Modulate DPT, Estrada-gomez S, Cardoso FC, Vargas-muñoz LJ, Quintana-castillo JC, Marcela C, Arenas G, Ste S, Saldarriaga-cordoba MM. *Toxins* (Basel) 2019;2019:496.
- [22] Hasan MM, Ragnarsson L, Cardoso FC, Lewis RJ. *PLoS One* 2021;16:1–18.
- [23] Wang D, Himaya SWA, Giacomotto J, Hasan MM, Cardoso FC, Ragnarsson L, Lewis RJ. *Mar. Drugs* 2020;18:1–13.
- [24] Xie XS, Van Deussen AL, Vitko I, Babu DA, Davies LA, Huynh N, Cheng H, Yang N, Barrett PQ, Perez-Reyes E. *Assay Drug Dev. Technol.* 2007;5:191–203.
- [25] Cardoso FC, Dekan Z, Smith JJ, Deuis JR, Vetter I, Herzig V, Alewood PF, King GF, Lewis RJ. *Br. J. Pharmacol.* 2017;174:2528–44.
- [26] Otvos RA, Heus F, Vonk FJ, Half J, Bruyneel B, Paliukhovich I, Smit AB, Niessen WMA, Kool J. *Toxicol* 2013;76:270–81.
- [27] Smith CF, Brandehoff NP, Pepin L, McCabe MC, Castoe TA, Mackessy SP, Nemkov T, Hansen KC, Saviola AJ. *Anal. Sci. Adv.* 2023;4:26–36.
- [28] Davis AP, Wieggers TC, Johnson RJ, Sciacy D, Wieggers J, Mattingly CJ. *Nucleic Acids Res* 2023;51:D1257–62.
- [29] Novak AE, Taylor AD, Pineda RH, Lasda EL, Wright MA, Ribera AB. *Dev. Dyn.* 2006;235:1962–73.
- [30] Kolesnikova TO, Demin KA, Costa FV, Zabegalov KN, de Abreu MS, Gerasimova EV, Kalueff AV. *Int. J. Mol. Sci.* 2022;23:1–18.
- [31] Panagides N, Jackson TNW, Ikonomopoulou MP, Arbuckle K, Pretzler R, Yang DC, Ali SA, Koludarov I, Dobson J, Sanker B, Asselin A, Santana RC, Hendrikx I, van der Ploeg H, Tai-A-Pin J, van den Bergh R, Kerckamp HMI, Vonk FJ, Naude A, Strydom MA, Jacobsz L, Dunstan N, Jaeger M, Hodgson WC, Miles J, Fry BG. *Toxins* (Basel) 2017;9.
- [32] Khan MA, Kerckamp HMI, de Bakker M, Fry BG, Richardson MK. *Toxicol* 2020; 177:S37–8.
- [33] Ali S, van Mil HGJ, Richardson MK. *PLoS One* 2011;6.
- [34] Still KBM, Nandlal RSS, Slagboom J, Somsen GW, Casewell NR, Kool J. *Toxins* (Basel). 2017;9:1–16.
- [35] Arrahman A, Kazandjian TD, Still KBM, Slagboom J, Somsen GW, Vonk FJ, Casewell NR, Kool J. *Toxins* (Basel). 2022;14:736.

- [36] Kramer S, Kotapati C, Cao Y, Fry BG, Palpant NJ, King GF, Cardoso FC. *Toxicol X* 2024;21:100184.
- [37] Dasgupta S, Reddam A, Liu Z, Liu J, Volz DC. *Environ. Pollut.* 2020;256.
- [38] Chahardehi AM, Arsad H, Lim V. *Plants* 2020;9:1–35.
- [39] Mladic M, de Waal T, Burggraaff L, Slagboom J, Somsen GW, Niessen WMA, Manjunatha Kini R, Kool J. *Anal. Bioanal. Chem.* 2017;409:5987–97.
- [40] Otvos RA, Mladic M, Arias-Alpizar G, Niessen WMA, Somsen GW, Smit AB, Kool J. *J. Biomol. Screen.* 2016;21:459–67.
- [41] Zietek BM, Mayar M, Slagboom J, Bruyneel B, Vonk FJ, Somsen GW, Casewell NR, Kool J. *Anal. Bioanal. Chem.* 2018;410:5751–63.
- [42] Gerlai R. *J. Neurosci. Methods* 2014;234:54–8.